A Bayesian-based approach for inversion of earth pressures on in-service underground structures

Zhiyao Tian[1,2], Shunhua Zhou[1,2], Anthony Lee[3], Yu Zhao[1,2], Quanmei Gong[1,2*]

[1] *Shanghai Key Laboratory of Rail Infrastructure Durability and System Safety, Tongji University, Shanghai, China*

[2] *Key Laboratory of Road and Traffic Engineering of the Ministry of Education, Tongji University, Shanghai, China*

[3] *School of Mathematics, University of Bristol, Bristol, United Kingdom*

**Corresponding author, E-mail address: gongqm@tongji.edu.cn. (Quanmei Gong)*

Abstract: This paper presents a Bayesian inversion approach to identify earth pressures on in-service underground structures based on structural deformations. Ill-conditioning and non-uniqueness of solutions are major issues for load inversion problems. Traditional approaches are mostly based on an optimization framework where a smooth solution is uniquely determined using regularization techniques. However, these approaches require tuning of regularization factors that may be subjective and difficult to implement for pressure inversion on in-service underground structures. By contrast, the presented approach is based on a Bayesian framework. Instead of regularization techniques and corresponding tuning procedure, only physically plausible bounds are required for specifying constraints. The complete posterior distribution of feasible solutions is obtained based on Bayes' rules. By inferring the potential pressures with the complete posterior distribution, a natural regularization advantage can be shown. Specifically, this advantage is demonstrated in detail by a series of comparative tests: *i*) the Bayesian posterior mean exhibits an inherent quality to smooth out ill-conditioned features of inversion solutions; *ii*) satisfactory inference of the pressures can be made even in the presence of non-uniqueness. These properties are valuable when observed data is noisy or limited. A recorded field example is also presented to show effectiveness of this approach in practical engineering. Finally, deficiencies and potential extensions are discussed.

Keywords: Earth pressures; Underground structures; Inversion problem; Load identification; Bayesian inference

1 Introduction

Due to the complexity of the urban underground environment, earth pressures on many in-service underground structures may exceed values expected in the design stage. As a result, excessive deformation and subsequent structural defects can occur, posing a threat to safety. For example, in soft soil areas, a number of shield tunnel structures were disturbed by nearby construction activities. The additional load from the disturbances has resulted in gross distortion of the tunnel linings [1−2], leading to severe leakage and segment cracks.

Identification of current earth pressures is crucial for health monitoring and performance prediction of such structures. For example, digital modeling, internal force estimation, or residual bearing capacity evaluation of the in-service structures requires a clear understanding of the current load state. However, direct measurement of the pressures by measuring devices can be rather difficult due to economic, technical, and logistical limitations [3−4]. By contrast, inversion of the load pressures based on easily observed structural responses, say deformation [5], is desirable.

Inversion of the design load on well-performing underground structures is straightforward [6]. The distribution of pressures can be assumed according to a design mode, see an example in Fig. 1(a). Consequently, the unknown parameters are restricted to specific unknowns on the load mode, e.g., vector $\mathbf{x}$ in Fig. 1(a), where $\mathbf{x}=(x_1,x_2,x_3)$. This parameterization enables the unknown pressures to be expressed as specific parameters on a particular load mode. By searching within this restricted parameter space, a good solution can be uniquely determined by minimizing the loss function between the observed structural response and that predicted by a forward model:

$$\begin{aligned} &\mathbf{x}_{\mathrm{d}} = \arg\min_{\mathbf{x}} \|\mathbf{d}-\mathbf{g}(\mathbf{x})\|_2^2, \\ &s.t. \quad h(\mathbf{x}) \le 0 \end{aligned} \tag{1}$$

where $\mathbf{x}_{\mathrm{d}}$ is the inversion result; $\mathbf{d}$ is the observed structural responses, say deformation; $\mathbf{g}(\mathbf{x})$ is called the forward model that maps any load parameters $\mathbf{x}$ into a predicted structural response; $h(\mathbf{x})$ is the potential constraints imposed on the parameters.

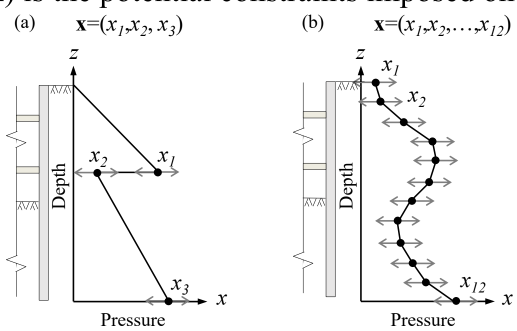

Fig. 1. Illustration example of the parameterization methods: (a) parameterization by assuming a design mode, e.g., according to Rankine's theory; (b) parameterization with an interpolation function

However, for in-service structures, the current load states may have already exceeded expected design mode and may be unevenly distributed [7−8]. In this case, Gioda and Jurina [9] used an interpolation function to approximate the unknown pressures. The function is the product of an interpolating matrix and unknown coefficients. In this way, the unevenly distributed pressures have been parameterized by a set of unknown coefficients, e.g., $\mathbf{x}=(x_1,\ldots,x_{12})$ in Fig. 1(b).

Gioda and Jurina's method [9] abandons design mode assumption on the pressures, which relaxes the inversion parameter space. However, without a strong restriction on the inversion parameter space (such as the design mode assumption), two significant issues can be introduced into the inversion problem, i.e., non-uniqueness and ill-conditioning [10−12]. That is, vastly different load states can give rise to predicted data that fit equally well with the observation data (due to an underdetermined mapping from $\mathbf{d}$ to $\mathbf{x}$), and a small error in the observed data may cause a large bias in the inversion result (due to the large condition number of the mapping from $\mathbf{d}$ to $\mathbf{x}$). Liu et al. [13] and Liu et al. [14] have observed this, and employed regularization techniques to impose regularized constraints on the parameter space to penalize undesired components, resulting in a smooth and unique solution. Among the regularization techniques, Tikhonov regularization has become the most widespread [15], which introduces a regularization term into Eq. (1):

$$\begin{aligned} &\mathbf{x}_{\mathrm{d}} = \arg\min_{\mathbf{x}} \{\|\mathbf{d}-\mathbf{g}(\mathbf{x})\|_2^2 + \gamma_r \|\mathbf{L}\mathbf{x}\|_2^2\} \\ &s.t. \quad h(\mathbf{x}) \le 0 \end{aligned}, \tag{2}$$

where γ_r is called the regularization factor, $\mathbf{L}$ is the s-th order derivative operator of $\mathbf{x}$ and s is usually chosen as 0, 1, or 2 [14]. The regularization term constrains the norm of $\mathbf{Lx}$ to be small. This makes Eq. (2) favor solutions that are relatively flat or smooth, thereby dealing with ill-conditioning. However, tuning suitable values of γ_r to obtain a satisfactory solution can be challenging [10, 16], relying heavily on the researchers' experience. It is also worth noting that both Eq. (1) and Eq. (2) are based on a deterministic framework to determine a unique solution using optimization algorithms. To the authors' knowledge, the non-uniqueness of solutions has hardly been discussed in the context of load inversion problems for underground structures.

Bayesian inference casts the inversion into statistical framework, where the output is the posterior distribution of the parameters that quantifies the ambiguity of all potential feasible solutions. Consequently, Bayesian inference have been used for uncertainty quantification in various fields such as soil parameter estimation [17−19] and defects identification [20] in geotechnical engineering. However, it has not been introduced to load inversion problems for underground structures. Although similar research has been conducted in identifying dynamic point loads on mechanical systems, these studies typically assume a Gaussian prior for the unknown parameters [21−23]. Under this assumption, the maximum *a posteriori* (MAP) solution in Bayesian approach is equivalent to the Tikhonov-regularized solution (i.e., Eq. 2) [10, 23], which enables the handling of ill-conditioning. Nevertheless, applying this assumption to load parameters of in-service underground structures can be very difficult and subject, as their values may already exceed expectations in the design stage. Furthermore, to avoid heavy computations, a MAP solution is typically chosen as a final result in Bayesian methods in this context [24]. To the best of the authors' knowledge, advantages of making statistical inference with the complete posterior distribution have not been shown yet.

In this paper, a Bayesian-based inversion approach for pressure identification on in-service underground structures is presented that does not require regularization techniques, Gaussian priors, or a corresponding tuning procedure. Based on an efficient Markov Chain Monte Carlo (MCMC) algorithm, the complete posterior distribution of inversion pressures is obtained. This approach encourages one to make inference with the complete posterior distribution whereby a natural regularization can be shown. Section 2 introduces this Bayesian load inversion approach in detail; Sections 3 presents its natural advantages in dealing with ill-conditioning and non-uniqueness; In Section 4, a recorded field example is carried out to show its effectiveness in practical engineering. Finally, deficiencies and potential extensions are discussed.

2 The Bayesian load inversion approach

2.1 Parameterization

Most mechanical problems of underground structures can be simplified as a plane strain problem, which is mainly the case discussed in this paper. Use z to represent a generalized coordinate on a structure, such as depth on a diaphragm wall or polar angle on a shield tunnel ring. The actual pressure field $Q(z)$ in the structural domain can be approximated as an unknown function $q(z)$. To avoid imposing erroneous constraints on the unknown pressures, Gioda and Jurina's method [9] is employed, which entails determining $q(z)$ as the interpolation of a series of unknown load parameters $\mathbf{x}=(x_1,x_2,\ldots,x_n)^{\mathrm{T}}$ located at control nodes $\mathbf{z}=(z_1,z_2,\ldots,z_n)^{\mathrm{T}}$ (Eq. 3, illustration example seen in Fig. 2(a)). Once the interpolation number n and nodes location $\mathbf{z}$ have been pre-defined, approximated pressure field $q(z)$ will be uniquely determined by $\mathbf{x}$. As a result, the inversion of the pressures has been transferred into the inversion of the intermediate parameters $\mathbf{x}$.

$$Q(z) \approx q(z) = \mathbf{I_z}(z)\mathbf{x}, \tag{3}$$

where, $\mathbf{I_z}(z)$ is the interpolating vector that can be varied according to the interpolation type, but the linear interpolation is often preferred by the researchers due to its simplicity and flexibility [9, 13−14] (its interpolating vector is presented in Appendix A).

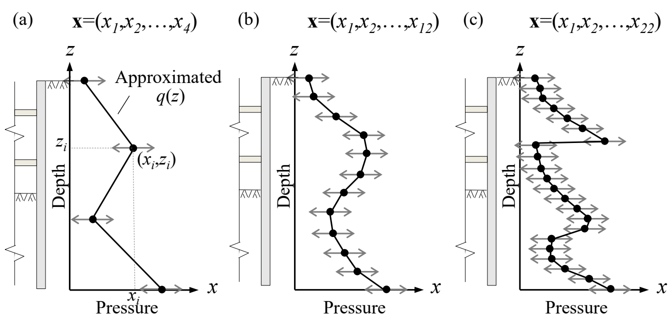

Fig. 2. Illustration example of the interpolation parameterization: (a) 4 parameters; (b) 12 parameters; (c) 22 parameters

The approximation capacity of q, with parameters $\mathbf{x}$, depends on the number n and locations $\mathbf{z}$ of the nodes. When no judgement can be made on the load distribution beforehand, it is recommended to place the nodes evenly on the structure. As for n, shown in Fig. 2(a)−(c), the more parameters (the denser nodes), the stronger the approximation capacity. As long as there are enough parameters, any pressure field can be approximated well. On the other hand, it is statistically and computationally more efficient to use less parameters. Although there is currently no widely accepted guideline for choosing node density in previous literatures, this study provides an example to illustrate a practical method for selecting an appropriate node density in section 4.

2.2 Bayesian framework for the load inversion problem

The unknown pressure field q has been parameterized by the load parameters $\mathbf{x}$. In a Bayesian inversion, inferences about the parameters are made using conditional probability given observed data according to Bayes' rule:

$$p(\mathbf{x}|\mathbf{d}) = \frac{p(\mathbf{d}|\mathbf{x})p(\mathbf{x})}{p(\mathbf{d})}, \tag{4}$$

where $p(\mathbf{x}|\mathbf{d})$ is the probability density of parameters $\mathbf{x}$ given the field data $\mathbf{d}$ (the observed deformations); $p(\mathbf{x})$ is the prior density of $\mathbf{x}$; $p(\mathbf{d}|\mathbf{x})$ is the likelihood function; $p(\mathbf{d})$, called "marginal likelihood", is a normalizing factor which makes $p(\mathbf{x}|\mathbf{d})$ integrate to one, and it can typically be ignored in the numerical estimation process of the posterior distribution.

2.2.1 The prior distribution

The prior distribution reflects one's prejudgment on the load parameters before obtaining data. Priors can have a strong influence on the posterior in a limited data setting [21, 25]. Improper prior can cause problems in practice, e.g., there is no guarantee that the posterior is even well-defined. Accordingly, it is preferable to ensure that the prior permits solutions that are plausible while allowing the data to strongly influence the posterior.

The load parameters are assumed to be uncorrelated before obtaining the data. Accordingly, $\mathbf{x}$ is considered as an independent random vector, and the prior distribution can be written as:

$$p(\mathbf{x}) = \prod_{i=1}^{n} p(x_i). \tag{5}$$

As for $p(x_i)$ (i=1,…,n), three typical priors are summarized and discussed as follows:

i) Completely flat prior: little judgement about the parameters can be made before inversion. In this case, the prior density of the parameters can be set to be completely flat: $p(x_i)=1$(i=1,…,n). Although such an improper prior [26] is not necessarily uninformative, it is objective, to some degree, in engineering practice when no information is available.

ii) Bounded uniform prior: generally, it is reasonable to set bounds for the parameters according to engineering judgment [9]. The bounds can help filter out some obviously unreasonable results while little judgement can be made on any values within the bounds. In this situation, the prior distribution of the parameters can be set as a uniform distribution within a physically plausible bound, e.g., $x_i \sim$ Uniform ($b_{\min}$, $b_{\max}$) (i=1,…,n). Such a prior is informative due to constraints from the bounds. In general, it is not difficult to determine a physically plausible bound for the soil-structure interaction pressures based on geotechnical engineering judgements.

iii) Gaussian prior: the prior distribution is centred at a given value with a variance. By tuning a suitable value of these parameters, the posterior distribution can be regularized and then a smooth solution can be uniquely determined [22]. Such a prior is clearly fairly informative and will strongly influence the posterior especially when the variance is tuned to be small. However, when no valid information is available, the parameters may be chosen improperly, whereby unacceptable bias may be introduced to the results.

For the earth pressures on in-service underground structures, it seems relatively difficult to require corresponding centre and variance information in a Gaussian distribution beforehand. By comparison, a flat prior may be more reasonable. Noted that a physically plausible bound can also be available in practice for necessary constraints. For example, a lower bound of the soil-structure interaction pressure can be set as 0 since almost no traction can be exerted by the soil. Thus, a bounded uniform prior is recommended in this approach. The bounds can be determined on a case-by-case basis according to reasonable geotechnical engineering judgements. However, it can be possible in some cases that one's engineering judgements on the bounds can be extremely weak. In this regard, determination of the bounds will be discussed in detail in section 4.3.

2.2.2 The likelihood function

The likelihood function measures the fit between observed deformation data and that predicted with a particular set of load parameter **x**, which is determined by the magnitude of error vector:

$$\mathbf{e} = \mathbf{d} - \mathbf{g}(\mathbf{x}), \tag{6}$$

where **d** is the observed deformation data; **g**(**x**) is the forward modelling function which returns a vector of predicted deformation data under the specific pressure field q (determined by the load parameters **x**, Eq. 3). The error vector **e** arises from inaccuracies in forward modelling (model error) and measurement error in observed deformations. In many cases, it is reasonable to assume that the model error is negligible when compared to measurement error (this will be discussed further in section 4.4). Given this assumption, as supported by the Central Limit Theorem, a zero-mean Gaussian distribution is typically assumed for the error distribution. The likelihood function is then

$$p(\mathbf{d}|\mathbf{x}) = p(\mathbf{g}(\mathbf{x}) + \mathbf{e}|\mathbf{x}) = p(\mathbf{e}|\mathbf{x}) = p(\mathbf{e}) = \frac{1}{(2\pi\bar{\sigma}_e^2)^{H/2}}\exp(-\frac{\mathbf{e}^{\mathrm{T}}\mathbf{e}}{2\bar{\sigma}_e^2}), \tag{7}$$

where H is the length of vector **e**, $\bar{\sigma}_e$ is the estimated standard deviation of the data errors. $\bar{\sigma}_e$ can be estimated as an unknown parameter too in an advanced hierarchical Bayesian framework [21]. However, it is beyond the scope of this paper. Since measurement instruments of the deformations can be generally known in advance, $\bar{\sigma}_e$ is determined according to the precision of measurement instruments in this paper.

2.2.3 The forward model

A forward model **g**(**x**) is required to compute the predicted deformation data under any given pressure field q (i.e., $\mathbf{I}_z(z)\mathbf{x}$, Eq. 3). As for the underground structures, it is commonly called load-structure model. For the convenience of solving the mostly higher order partial differential governing functions, finite element method (FEM) can be adopted:

$$\mathbf{g}(\mathbf{x}) = \mathbf{K}^{-1}\mathbf{f}(\mathbf{I}_{\mathbf{z}}(z)\mathbf{x}), \tag{8}$$

where the structure is discretized into a series of elements and **K** is the global stiffness matrix; **f** is a vector-valued function where $\mathbf{f}\,(\mathbf{I}_{\mathbf{z}}(z)\mathbf{x})$ is the equivalent nodal forces that are equivalent to the distributed pressures q (i.e., $\mathbf{I}_{\mathbf{z}}(z)\mathbf{x}$) with the transformation rules of virtual work. Here, for a better illustration, derivation of **K** and **f** for the most commonly used "Beam on elastic foundation" model, is presented in Appendix B. For a linear elastic case, the predicted deformation data can be computed directly with Eq. (8) while an iterative procedure will be required when considering the non-linear behaviour of the mechanical system, such as a Newton-Raphson Method.

2.2.4 Solution of Bayesian inversion

2.2.4.1 Maximum likelihood estimation or posterior means?

With a deterministic approach, it is reasonable to extract a solution uniquely from the posterior density, i.e., according to the prior and likelihood, the MAP estimate:

$$\mathbf{x}_{\mathrm{MAP}} = \arg\max_{\mathbf{x}} p(\mathbf{x}|\mathbf{d}) = \arg\max_{\mathbf{x}} p(\mathbf{d}|\mathbf{x})p(\mathbf{x}), \tag{9}$$

which can be obtained analytically. Table 1 presents the MAP solution of Bayesian inversion under three typical types prior information. The optimal solution in deterministic inversion under the same condition are also given in this Table.

It is found that when taking a completely flat prior, $p(x_i)=1(i=1,\ldots,n)$, the MAP in Bayesian inversion is equivalent to the optimal solution in an unconstrained deterministic inversion; Certainly, when taking a bounded uniform prior, i.e., $x_i \sim$ Uniform $(b_{\min}, b_{\max})$ $(i=1,\ldots,n)$, the MAP is also equivalent to the optimal solution in a deterministic inversion under the equivalent constraints $b_{\min}<x_i<b_{\max}$ $(i=1,\ldots,n)$; When taking a zero-mean Gaussian prior, i.e., $x_i \sim \mathrm{N}\,(0, \sigma_p^2)$ $(i=1,\ldots,n)$, the MAP is equivalent to the optimal solution in a deterministic inversion using Tikhonov regularization when **L** in Eq. (2) is determined as the 0-th order derivative operator.

It is known that ill-conditioning is a major issue in deterministic inversion. Thus, the same can be true for the MAP solution in Bayesian inversion. Although regularization techniques can be introduced to make the solution more well-behaved, this may introduce unacceptable bias.

Instead of choosing the MAP solution or the optimal solution in deterministic inversion, it is recommended to make an inference based on the entire posterior distribution. A natural regularization of Bayesian inversion (without regularization techniques) can be shown when inferring with the ensemble posterior solutions. Typically, the posterior mean/expectation of the parameters **x** or pressure field q at a given z are mathematically equivalent to:

$$E(\mathbf{x}|\mathbf{d}) = \int \mathbf{x}p(\mathbf{x}|\mathbf{d})d\mathbf{x}, \tag{10}$$

$$E(q(z)|\mathbf{d}) = \int \mathbf{I}_{\mathbf{z}}(z)\mathbf{x}p(\mathbf{x}|\mathbf{d})d\mathbf{x}. \tag{11}$$

Posterior means minimize expected squared loss, where the expectation is taken with respect to the posterior [26]. In a qualitive perspective, MAP is a solution that best fits the observation data and the noise in data as well. In addition to MAP, quantities of "less-fitted" ones that are insensitive to data noise are also considered as feasible solutions with corresponding probabilities. By averaging all the feasible solutions appropriately to obtain a posterior mean, the high-frequency features of any individual solution caused by observation errors can be flattened. This is described as the inherent smoothing quality of Bayesian inference [16]. The natural regularization will be shown directly in the following cases.

2.2.4.2 Estimation of the posterior distribution

As mentioned above, a Bayesian approach requires estimation of the posterior distribution. However, when the prior and posterior are not of the same distribution family, analytical solution of Eq. (4) can rarely be achieved. Alternatively, Markov Chain Monte Carlo (MCMC) is an effective numerical algorithm for estimating posterior distributions. The basic idea of MCMC is demonstrated as: i) Construct a transition kernel $P(t \rightarrow t+1)$ based on Detailed Balance [27]; ii) Sampling iteratively with $P(t \rightarrow t+1)$ to construct an ergodic Markov Chain whose stationary distribution is the posterior distribution.

Without constraints from a strong prior distribution, many iterations will be required for the chain to achieve convergence. Especially when computation of the forward model is computationally intensive, estimation of the posterior distribution can be a daunting task [28]. Thus, a more efficient MCMC algorithm called Differential Evolution Markov Chain (DE-MC) [29] is introduced to increase sampling efficiency. In DE-MC, N parallel "chains" are run simultaneously and "learn" from each other to tune the scale and orientation of the transition kernel adaptively, which shows good efficiency for approximating the posterior distribution. The transition kernel of DE-MC can be built according to:

i) generate a next proposal of the ith chain (i=1,…,N) after iteration step t based on Differential Evolution:

$$\mathbf{x}_p^i = \mathbf{x}_t^i + \lambda(\mathbf{x}_t^a - \mathbf{x}_p^b) + \zeta_n, \tag{12}$$

where λ is the jump rate; $\zeta_n \sim \mathrm{N}_n(0,c)$ is drawn from a normal distribution with a small standard deviation to ensure ergodicity; a and b are integer values drawn without replacement from set $\{1,\ldots,i\text{-}1,i+1,\ldots,N\}$.

ii) accept the proposal $\mathbf{x}_{t+1}^i = \mathbf{x}_p^i$ with probability p_{acc} ($x_t^i \rightarrow x_p^i$); and reject otherwise: $\mathbf{x}_{t+1}^i = \mathbf{x}_t^i$, where

$$p_{acc}(\mathbf{x}_t^i \rightarrow \mathbf{x}_p^i) = \min[1, \frac{p(\mathbf{x}_p^i|\mathbf{d})}{p(\mathbf{x}_t^i|\mathbf{d})}], \tag{13}$$

where Eq.(4) is adopted to estimate the ratio between $p(\mathbf{x}^i_p|\mathbf{d})$ and $p(\mathbf{x}^i_t|\mathbf{d})$. Accordingly, with the proposal function (Eq. 12) and accept ratio (Eq. 13), the Markov chain has a stationary distribution in which each of the N components are independent and distributed according to the posterior. After convergence of the chains, a set of posterior samples $\{\mathbf{x}_s, s=1,\ldots,S\}$, extracted from all the components, can be used to estimate the posterior distribution:

$$p(\mathbf{x}|\mathbf{d}) \approx \frac{1}{S}\sum_{s=1}^{S}\delta(\mathbf{x}-\mathbf{x}_s), \tag{14}$$

where, $\delta(\cdot)$ is the Dirac delta function. And the density of $q(z)$ can also be estimated as:

$$p(q(z)|\mathbf{d}) \approx \frac{1}{S}\sum_{s=1}^{S}\delta(q(z)-\mathbf{I_z}(z)\mathbf{x}_s)\,. \tag{15}$$

Hence, Eqs. (10) and (11) reduce to:

$$E(\mathbf{x}) = \frac{1}{S}\sum_{s=1}^{S}\mathbf{x}_s \tag{16}$$

$$E(q(z)) = \frac{1}{S}\sum_{s=1}^{S}\mathbf{I_z}(z)\mathbf{x}_s \tag{17}$$

Convergence of the Markov Chains can be monitored by the scale-reduction factor proposed by Gelman and Rubin [30]:

$$\sqrt{\hat{R}_i} = \sqrt{\frac{t_i-1}{t_i} + \frac{N+1}{Nt_i}\frac{B}{W}} \tag{18}$$

where, t_i is the number of iterations in the ith chain (i=1,…,N); N is the number of chains; B is the variance between chain means; W is the average of within-chain variances; and it is recommended that a value of $\sqrt{\hat{R}_i}$ less than 1.2 indicates convergence of the chain.

3 Advantages in dealing with non-uniqueness and ill-conditioning

A Numerical example was presented to demonstrate how to perform this approach on an underground structure. Most importantly, a series of comparative tests were carried out to illustrate the natural regularized property of this approach.

3.1 Preliminaries

For convenience of discussion, a linear elastic case is assumed here. A diaphragm wall bended towards a pit as a result of the active earth pressures behind it. The structure and soil properties are summarized in Fig. 3(a). The physical process can be simplified as beam, on elastic foundation, loaded by the pressures. Specifically, flexural rigidity of the wall EI is 2.5×10^6 kN•m^2, the foundation stiffness increases linearly with depth with a scaling factor m_2=5×10^3 kN/m^4. The "actual" pressure field was estimated according to Rankine's theory (Fig. 3(b)). The pressures, combined with the forward model (Eq. 8), generated a set of synthetic deformation data $\mathbf{d}$=(d_1,…,d_{41}) (measuring every 0.5 m on the wall, seen in Fig. 3(c)). Then, the objective is inversion of the actual pressures (assumed unknown now) based on the synthetic data (in some cases, contaminated by a set of random noise $\boldsymbol{\varepsilon}$ to simulate the observation errors).

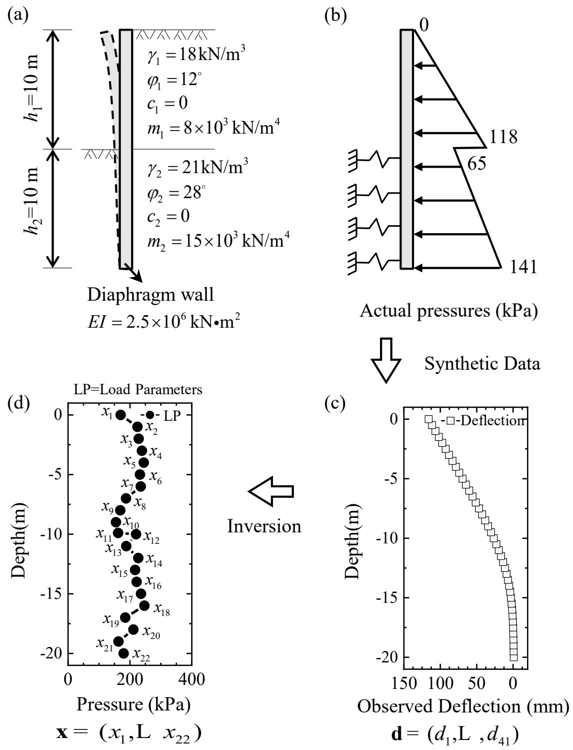

Fig. 3. The numerical example: (a) a diaphragm wall bends towards a pit; (b) assumed actual earth pressures acting on the wall; (c) synthetic deflection data generated by the assumed pressures; (d) parameterization with 22 unknown load parameters. ((Note: γ=unit weight; φ=friction angle; c=cohesion; m=scaling factor of the foundation stiffness; EI=flexural rigidity)

Firstly, unknown parameters were taken with a dense grid (1 m apart) in the structural domain. Since it is generally known *a priori* that an abrupt change of active earth pressures can occur on the soil interface (depth = −10 m), an additional unknown factor was added at the interface. Thus, 22 unknown parameters $\mathbf{x}=(x_1,\ldots,x_{22})$ were set, shown in Fig. 3(d).

As for the prior distribution of these parameters, from the engineering judgement, lateral active earth pressures on the wall must be positive and within a limited bound, say the self-weight stress of soil at the wall bottom $\gamma_1 h_1+\gamma_2 h_2\approx 400$ kPa. Thus, a bounded uniform prior was set as $x_i\sim$ Uniform (0,400) (i=1,…,22).

For the likelihood function, assume that precision of measurement was known in advance (see discussion in section 2.2.3). Thus, $\bar{\sigma}_e$ was determined equal to the standard deviation of the added noise (in a noiseless case, a very small value, i.e., 10^{-5} was adopted).

With the sampling algorithm introduced in section 2.2.4.2, ergodic Markov chains can be simulated that will converge to the posterior distribution. According to Ter Braak [29], the number of components N should be at least $2n$ (n is number of the parameters). As a result, N was taken to be 44 and the number of iterations was set to be 20000.

For the necessary comparison, cases were set as follows. *i*) Case 1: observed data for input were the original deformations $\mathbf{d}$, assuming that the observation was perfect and no errors exist. *ii*) Cases 2: observed data for input were contaminated deformations $\mathbf{d}+\boldsymbol{\varepsilon}$, where the noise is Gaussian-distributed to simulate the measurement errors (with a standard derivation of 1 mm). For robustness testing, there different sets of random noise were set, i.e., $\boldsymbol{\varepsilon}_1 \sim$ N (0,1) for case 2-1 (Fig. 4a), $\boldsymbol{\varepsilon}_2 \sim$ N (0,1) for case 2-2 (Fig. 4b), and $\boldsymbol{\varepsilon}_3 \sim$ N (0,1) for case 2-3 (Fig. 4c).

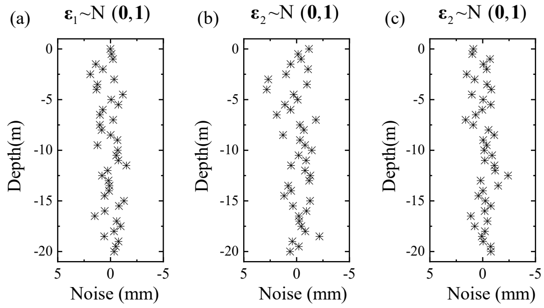

Fig. 4. Noise to contaminate the observed deformations: (a) case 2-1; (b) case 2-2; (c) case 2-3.

For comparison, an accompanying deterministic inversion (Eq. 1) was run for every case, respectively, with the same input data and equivalent bounded constraints mentioned in Table 1. Especially, a Tikhonov regularized deterministic inversion (using the equation in Table 1) was also run for cases 2, discussed in the last.

To evaluate how well the inversion results fit the actual pressures, coefficient of determination R^2 is introduced:

$$R^2 = 1 - \frac{\sum_{j=1}^{M_p} [q_A(z_j) - q_I(z_j)]^2}{\sum_{j=1}^{M_p} [q_A(z_j) - \frac{1}{M_p}\sum_{j=1}^{M_p} q_A(z_j)]^2}, \tag{19}$$

where, $q_A(z_j)$ is the actual pressure at a monitoring point z_j, $q_I(z_j)$ is the inversion pressure at z_j, the monitoring points are chosen dense enough in the structural domain (every 0.2 m in this case), and M_p is the number of the points. Generally, R^2 ranges from 0 to 1, and the closer R^2 is to 1, the closer the inversion result is to the actual values. But when the inversion results are extremely poor, R^2 can yield negative values [31]. In this case, negative values are modified to 0 indicating a complete failure of an inversion.

3.2 Results

Take case 1 as an example to present the sampling process. As seen in Fig. 5, the scaling-reduction factors of the 22 parameters $\sqrt{\hat{R}_i}\ (i=1,\ldots,22)$ quickly converged to be less than the threshold value 1.2 within 5000 steps, indicating that the components were close to their stationary distribution. The last 50% of the samples in the chain were used to estimate the posterior distribution.

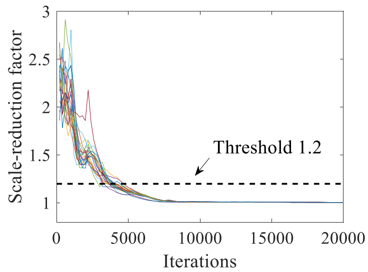

Fig. 5. Evolution of scale reduction factors for all parameters

The posterior distribution for $q(z)$ was estimated by Eq. (15), and visually presented in Fig. 6(a). Estimated probability density of pressures at every point of the wall is illustrated by different color levels quantitatively. More intuitively, for example, the posterior densities of pressures at points A, B, and C are presented in Fig. 6(b). More importantly, posterior mean of the pressure field was also estimated (Eq. 17) to make an inference of the actual pressures. The actual pressures and posterior mean (PM) pressure field obtained by Bayesian inversion are presented in Fig. 6(c). Besides, the optimal solution (OS) obtained by deterministic inversion is also presented in this figure. It is found that both of the two results fit perfectly with the actual pressures. Simultaneously, R^2 of the two inversions are 1.00, indicating both of Bayesian inversion and Deterministic inversion are effective in this extreme case where the observation is perfect and no errors contaminate the input data.

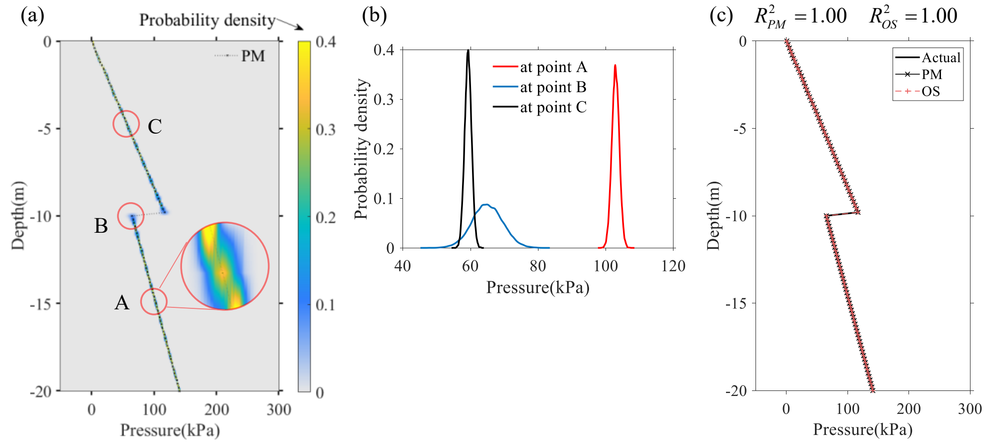

Fig. 6. Inversion results of case 1: (a) marginal posterior densities of pressure field on the structure; (b) posterior densities of pressure at Points A, B, and C (illustration example); (c) comparison between the actual pressures and inversion results obtained by Bayesian and deterministic inversion. (Note: PM=posterior mean obtained by Bayesian inversion; OS=optimal solution obtained by deterministic inversion).

3.3 Natural advantages

3.3.1 To deal with ill-conditioning

Then, the input observed data was contaminated by measurement errors, i.e., cases 2. For deterministic inversion, as shown in Figs. 7(a)−(c), although the inversion results are constrained in the bound of 0−400 kPa, dramatic fluctuation occurs on the overall pressure field. In addition, the inversion results do not fit with the actual pressures at all (R^2_{OS}=0 in all the three cases). It can be identified as a typical ill-conditioned problem (or "over-fitting" to measurement errors), i.e., due to the large condition number of the stiffness matrix **K** (in Eq. 8), a small error in the deformation measurement leads to a large bias in the inversion pressures. Compared with the optimal solution (OS) by deterministic inversion, the posterior means (PM) by Bayesian inversion seems to be much smoother. In addition, the PM fit relatively well with the actual pressures in the cases (with R^2_{PM}=0.85 in case 2-1, R^2_{PM}=0.89 in case 2-2, and R^2_{PM}=0.87 in case 2-3). This is the so-called natural regularization of Bayesian estimation. That is, the posterior means flatten the "over-fitting" features of individual solutions. What's more, the relatively stable posterior means present in the three cases have also shown robustness of this approach.

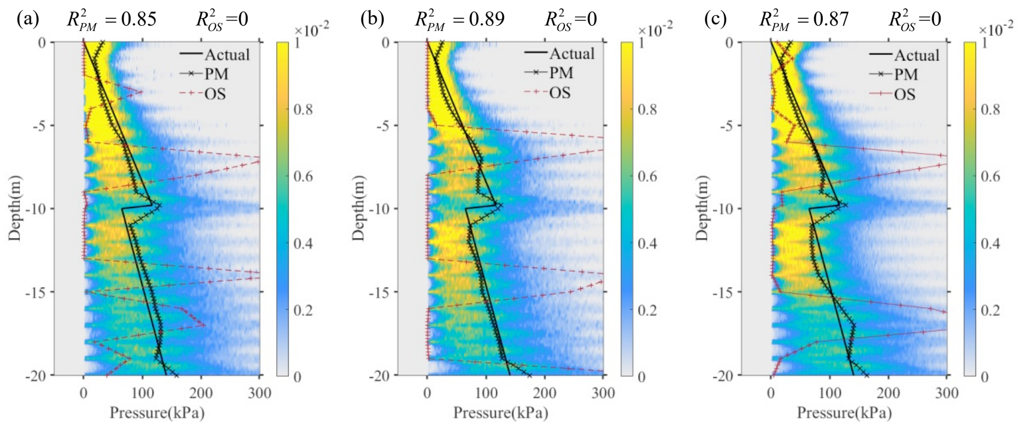

Fig. 7. Inversion results: (a) case 2-1; (b) case 2-2; (c) case 2-3. (Note: PM=posterior mean obtained by Bayesian inversion; OS=optimal solution obtained by deterministic inversion).

Admittedly, there are regularization techniques introduced in deterministic inversion to treat ill-conditioning. Inversion results of Tikhonov-regularized deterministic inversion with different regularization factor γ_r are presented in Figs. 8(a)−(c). It is found that when γ_r is getting larger, the inversion results are getting smoother, but the results are more closed to predefined centre values and fit poorly with the actual pressures. It is difficult to tune this factor to obtain satisfactory results. By comparison, this Bayesian-based approach requires no regularization techniques but simultaneously shows “natural” regularization property, which is valuable.

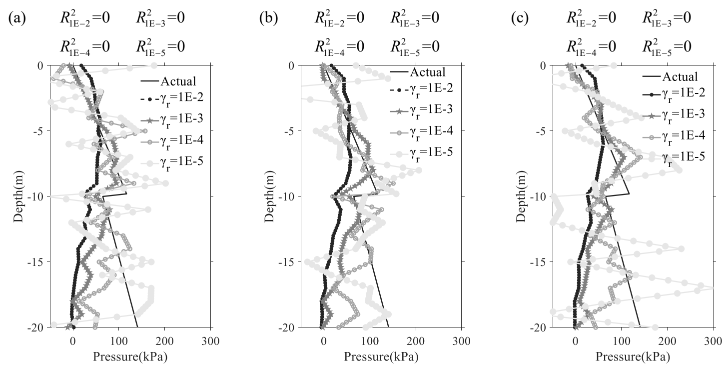

Fig. 8. Inversion results obtained by deterministic inversion with the help of Tikhonov regularization while tuning the regularization factor γ_r: (a) case 2-1; (b) case 2-2; (c) case 2-3.

3.3.2 To deal with non-uniqueness

Without a strong regularization, deterministic inversion may be faced with non-uniqueness, i.e., vastly different solutions can fit equally well observed data. It is especially the case when the number of unknown parameters is more than the number of observed data so that inversion of Eq. (8) can be underdetermined [13−14]. Nevertheless, non-uniqueness is natural in Bayesian inversion and can be quantified with probabilities which can aid robust decision-making.

On basis of case 1, three cases are carried out where the number of input observed data are 11 (observing every 2 m, seen in Fig. 9a, case 3-1), 6 (observing every 4 m, seen in Fig. 9b, case 3-2), and 3 (observing every 10 m, seen in Fig. 9c, case 3-3), while the unknown parameters keeps unchanged (22 parameters). Without regularization techniques, deterministic inversion cannot be achieved in these cases since the number of unknown parameters is much larger than the number of the observed data [9]. But the posterior distribution can still be obtained by Bayesian inversion (Figs. 10(a)−(c)). As for cases 3-1 and 3-2, the number of unknown parameters is 2 and 3.5 times that of the observed data. It is found that the posterior means (PM) fits relatively well the actual pressures ($R^2{}_{PM}$=0.95 and $R^2{}_{PM}$=0.87, respectively), indicating that Bayesian inversion is still effective in this situation. Of course, with less observation data, the more uncertain the result and this is reflected in the posterior distribution. Comparison between Figs. 10(a)−(c) shows that as the amount of observed data decreases, the posterior densities become more flat ("hot areas" reduce) and the fitness of the posterior mean decreases, although the actual pressure field remains within the shaded region with significant posterior probability. Thus, if available, it is encouraged to collect more data to achieve a better inversion result.

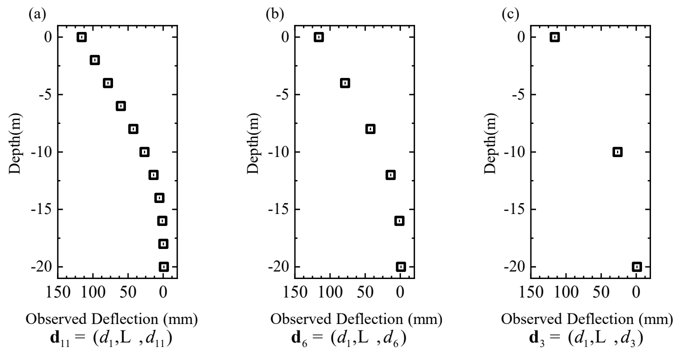

Fig. 9. Input observed data for cases 3 where the number of unknown parameters is more than the observed data: (a) case 3-1; (b) case 3-2; (c) case 3-3.

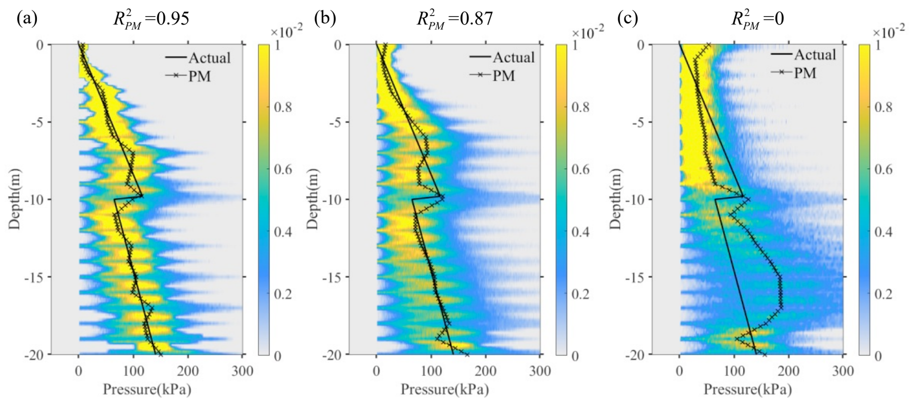

Fig. 10. Inversion results obtained by Bayesian inversion in cases 3: (a) case 3-1; (b) case 3-2; (c) case 3-3. (Note: PM=posterior mean obtained by Bayesian inversion).

It is noting that according to a statistical thinking, the inversion results of Bayesian inversion are not limited to the posterior mean. It can be more appropriate to make inference with the complete posterior distribution. For example, with posteriors of pressures in Figs. 10(a)−(c), probability densities of internal forces at any points on the wall were further derived seen in Figs. 11(a)−(c). With these probability densities, statistics inferences, such as expectation of maintenance cost, can be estimated to make a more robust engineering decision, which is not possible using a deterministic inversion.

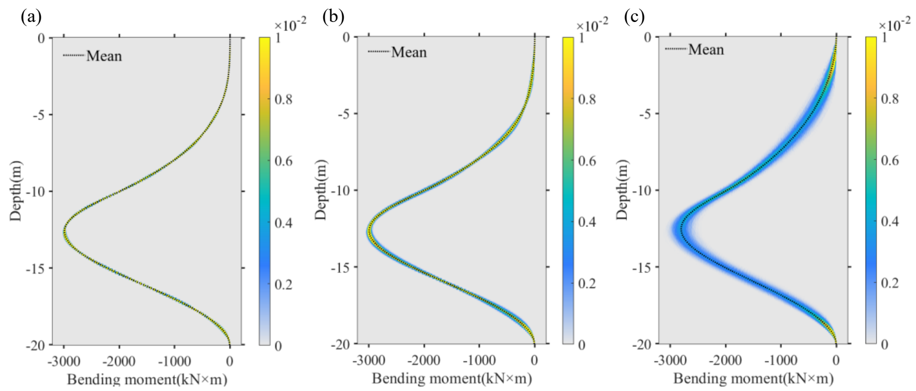

Fig. 11. Estimated probability densities of bending moment on the wall in cases 3: (a) case 3-1; (b) case 3-2; (c) case 3-3.

4 Application in engineering practice

A field data example is carried out to verify effectiveness of this approach in practical engineering as well as to stimulate discussion on the future extensions.

4.1 Preliminaries

A filed case was recorded in detail in Smethurst and Powrie [32] that a pile bend under loads imposed by a slope (Fig. 12(a)). Displacements on the pile were measured by inclinometer tubes cast into the pile (Fig .12(b)). Thus, the objective is inversion of the net earth pressures acting on the pile based on the inclinometer measurement and comparation with the net earth pressures recorded in this literature which are deduced from the strain gauges data.

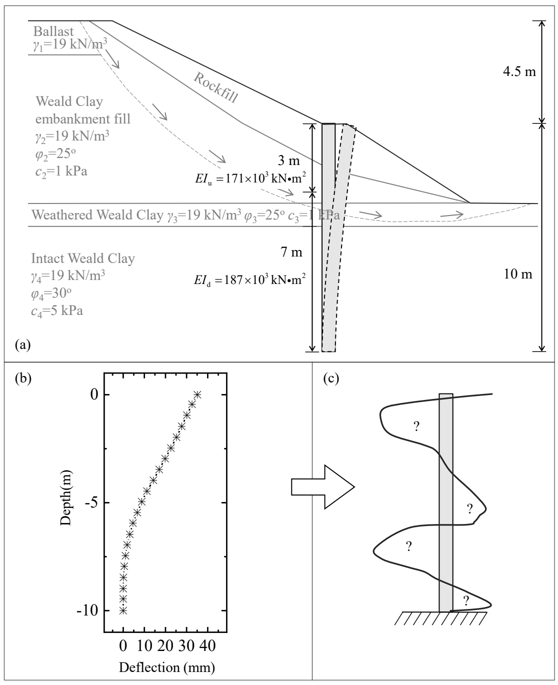

Fig. 12. The field example recorded by Smethurst and Powrie [32]: (a) a pile bends in a slope; (b) observation deflection on the pile; (c) simplified as a cantilever beam.

According to Smethurst and Powrie[32], the pile base was installed into the intact Wealed Clay, which tightly held the lower portions of the pile. Moreover, displacement data indicated that there was no movement or rotation at the pile base. Consequently, the physical process was assumed to be that of a cantilever beam, subjected to unknown net pressures due to slope movement, and bending towards the slope toe (Fig. 12(c)). The forward model of a cantilever beam can be easily obtained by deleting the foundation reaction term from the beam on elastic foundation model (Appendix B), and set a fixed end at the pile base.

As a result of the slope, distribution of the pressures can be very complex, which may lead to a difficult parameterization. However, as mentioned in section 2.1, the more parameters, the stronger the approximation capacity. In particular, with evenly spaced nodes, as the number of parameters increases, the actual pressures can ultimately be approximated arbitrarily well. Thus, a series of pilot calculation were carried out for a trial. Parameters were set evenly on the pile, while the number of parameters n kept growing to monitor a convergence of the inversion results (Table 2).

For the prior distribution, as the underlying stratum held the pile bottom perfectly, it was assumed that the net pressures were less than the self-weight stress of soil at the pile bottom, i.e., about 300 kPa (a rough calculation of 20 kN/m^3 × 14.5 m). Accordingly, the prior distribution of the parameters was set as $x_i \sim$ Uniform(-300,300) (i=1,…,n) (setting of this prior will be discussed in detail later in section 4.3). According to the precision of measurement instrument [32], $\bar{\sigma}_e$ in the likelihood function is determined to be 1 mm. Similar to the numerical example, 2n components are run in DE-MC algorithm and the number of iterations is set to 10000.

4.2 Results

Posterior densities of the pressure field on the pile in calculations A−F are presented in Figs. 13(a)−(f), respectively. As seen in Figs. 13(a)−(c), when the number of parameters is relatively small, due to insufficient parameterization capacity, the shape of the posterior means (PM) seems to be simple. But with more parameters, the shape of the posterior means becomes complex. As seen in Fig. 13(d)−(f), the posterior means (PM) seem to remain unchanged with the increase of parameters number. Simultaneously, posterior means (PM) in calculations A−F are plot in a same figure (Fig. 14). It is found that with the increase of parameters, the inversion results converged gradually. Especially, the posterior means of 15-parameters and 16-parameters almost coincided, indicating a stable result has been achieved, seen Fig. 13(f). Meanwhile the actual net pressures recorded in Smethurst and Powrie [32] are also presented in Fig. 13(f). In general, the posterior means (PM) fit quite well with the actual pressures with R^2_{PM}=0.71, indicating effectiveness of the Bayesian load inversion approach.

It is worth noting that the inversion pressures deviate from the actual pressures at the pile bottom to a certain extent. It can be attributed to the displacement constraint of the cantilever beam where deflection is not sensitive to the pressures at all. For comparison, deterministic inversion with an equivalent constraint was also run for this case. The inversion results by deterministic inversion are presented by the red line (OS) in Fig. 13(f). It is found that ill-conditioning made deterministic inversion failed again with R^2_{OS}=0. By contrast, Bayesian inversion proved to be a more effective approach in handing ill-conditioning in this case.

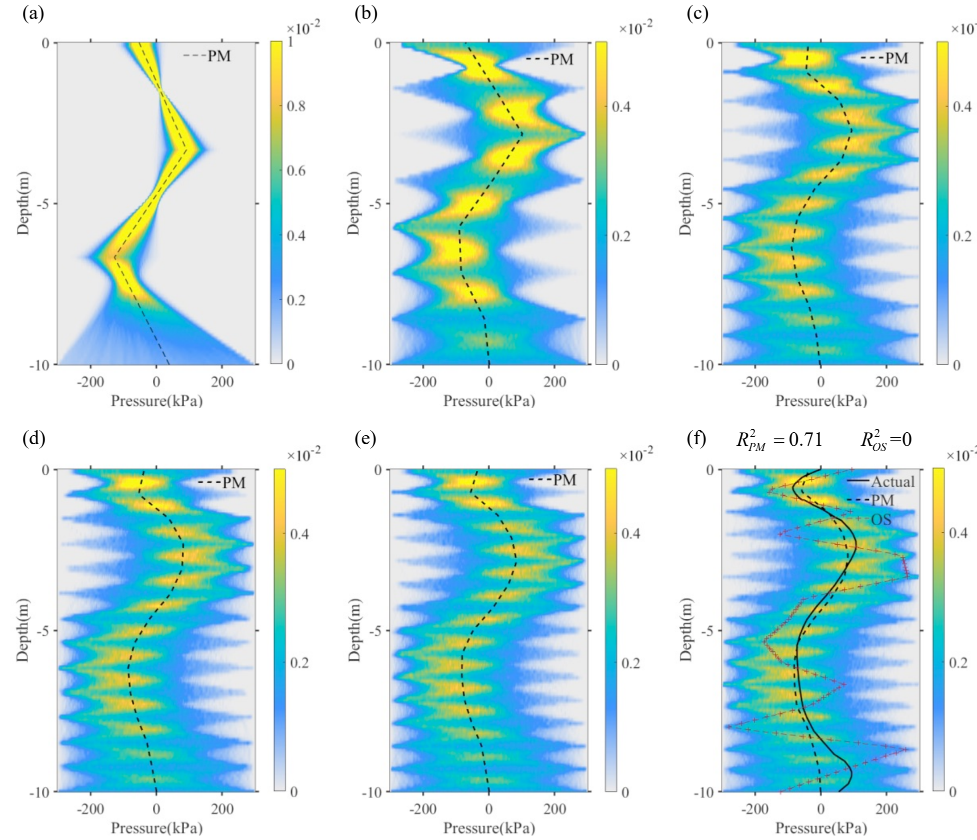

Fig. 13. Inversion results: (a) calculation A (4 parameters); (b) calculation B (8 parameters); (c) calculation C (12 parameters); (d) calculation D (14 parameters); (e) calculation E (15 parameters); (f) calculation F (16 parameters). (Note: PM=posterior mean obtained by Bayesian inversion; OS=optimal solution obtained by deterministic inversion).

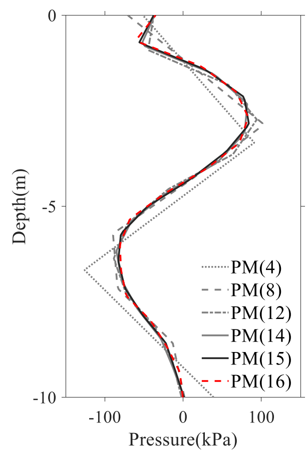

Fig. 14. Posterior means obtained by calculations A−F. (Note: PM(n)=posterior mean obtained in the n-parameters pilot calculation).

In order to explain the effectiveness of the proposed Bayesian approach, the posterior distribution of earth pressures, as depicted in Fig. 13(f), is utilized to drive the cantilever beam model to compute the pile displacement. As shown in Fig. 15, the measured displacement data fall within the computed 95% confidence interval and generally fits well with the posterior mean. However, it is important to note that the posterior mean does not fit each individual data point perfectly, as evidenced by an example at depth 5.9 m. This can be attributed to the fact that, unlike deterministic inversion, the Bayesian approach does not attempt to minimize the error vector in Eq. (6). Rather, it treats the errors as random variables, allowing both the best-fitted displacement and quantities of "less-fitted" ones to be considered feasible. By accurately averaging all feasible results, the posterior mean is smoothed out, thereby preventing overfitting to measurement errors and the subsequent emergence of ill-conditioned features in the earth pressures.

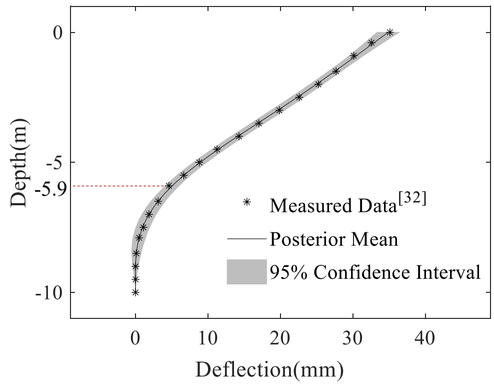

Fig. 15. The computed pile displacement and corresponding measurement data.

4.3 Robustness tests

It should be noted that regularization techniques are not required in this approach. However, as shown in the cases, a physically plausible bound is needed to specify parameter constraints. Accordingly, a doubt may arise that are the inversion results sensitive to the bounds? Specifically, how loose can the bounds be while retaining satisfactory performance, and what if the bounds are too narrow? Only if these questions are answered, can this approach be used with confidence in practical engineering.

In response to the first question, an extreme situation was assumed for this field case. Assumed that the pile bottom tended to deform towards the back of the slope. Due to the passive deformations, the soils were forced to be in a limited state. In this situation, net pressures on the pile might reach a limited passive pressure. The passive pressures on the pile bottom can be roughly estimated as $K_p \times 300$ kPa, where K_p is the coefficient of passive earth pressure that can be estimated as $K_p = \tan^2(45^{\mathrm{o}}+\varphi/2)$ [33] = $\tan^2(45^{\mathrm{o}}+30^{\mathrm{o}}/2) = 3$. Accordingly, the bound for constraints must be relaxed to be [-900, 900] kPa., Then effectiveness of this approach under the prior $x_i \sim$ Uniform(-900,900) (i=1,…,n) were tested here. It is worth mentioning again that [-900, 900] is extremely loose and redundant for this case, for the following three reasons. *i*) the soils were assumed to be in a passive limited state with a rupture surface extended to the ground surface; *ii*) K_p was estimated according to the fraction angle of intact weald clay that assumed all the strata were replaced by this stratum with the best engineering properties; *iii*) K_p was estimated according to Rankine's theory that assumed the slope was filled to be flat. For comparison, similar bounds of [-600, 600] and [-1200, 1200] kPa (2 and 4 times of the original bounds, respectively) were also tested here.

Inversion results under the bounds of [-600, 600], [-900, 900], and [-1200, 1200] kPa were presented in Figs. 16(a)−(c), respectively. Obviously, with the relaxation of the bounds, samples outside the original bound [-300, 300] kPa were accepted as feasible solutions as well that makes the posterior distribution more and more flat ("hot area" reduced). However, the posterior mean that represents the majority of feasible solutions was still capable of smoothing out ill-conditioning features of individual solutions. Although the accuracy of the posterior mean decreased with relaxation of the bounds, satisfactory inversion results could still be obtained in the extreme case, i.e. [-900, 900], with $R^2{}_{PM}$=0.66. By contrast, inversion results of deterministic inversion were getting more and more ill-conditioned with relaxation of the bounds. These tests demonstrate robustness of this approach in practical applications. That is, even when one's engineering judgement is very weak to determine the prior bounds (e.g., in the extreme case of [-900 900] kPa), satisfactory inversion results can still be obtained.

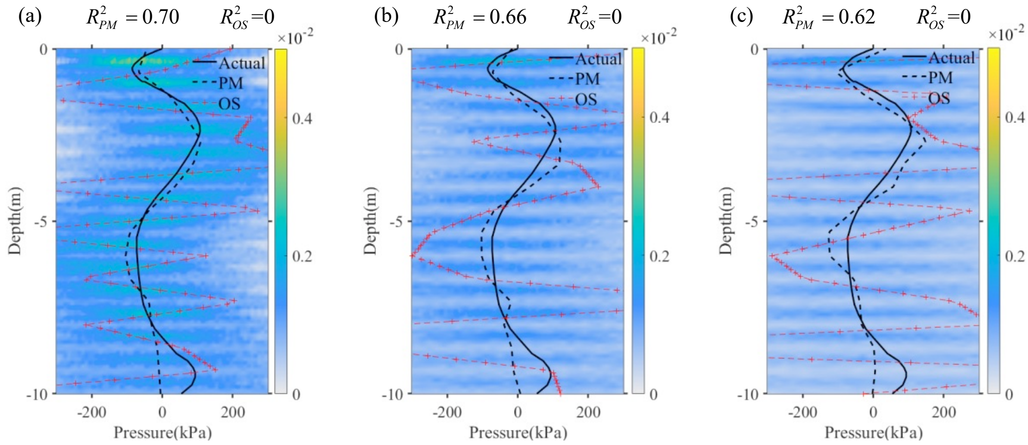

Fig. 16. Inversion results under different bounds: (a) [-600, 600] kPa; (b) [-900, 900] kPa; (c) [-1200, 1200] kPa. (Note: range of x-axis was set to be [-300, 300] kPa in all the figures since posterior mean is the main focus; PM=posterior mean obtained by Bayesian inversion; OS=optimal solution obtained by deterministic inversion).

In terms of the second question, choosing bounds that are too narrow can be dangerous. For instance, if the bound was determined to be [-50, 50] kPa for this case, the actual pressures cannot be identified. Most importantly, as the actual pressure will never be known in advance, how could one know whether a bound was determined to be too tight? One way to address this is to performance successive relaxation of the bounds and monitor whether the inversion results significantly differ each other and exceed the original bound. If yes, the original bound may be unreasonable. For example, in this case, when the original bound was relaxed from [-300, 300] to [-600, 600] kPa, the posterior means did not differ too much (Fig. 16a), suggesting that the choice of [-300, 300] kPa was reasonable.

4.4 Limitations and future Extensions

It should be noted that the testing cases did not consider the non-linear mechanical behavior of the structures. However, Smethurst and Powrie [32] have suggested that cracks may develop between 4.5 m and 8.5 m depth of the pile, which can result in a non-linear stiffness reduction of the concrete during the loading process. While the full uncracked stiffness was used for the inversion approach, it is important to consider whether this non-linear behavior would significantly affect the inversion results. To address this question, an extreme case (referred to as the "cracked case") was tested, where the cracked bending stiffness (75% of the uncracked value, according to

Smethurst and Powrie) was used between 4.5 m and 8.5 m depth of the pile throughout the entire loading process. All other conditions were kept the same as in Calculation F (referred to as the "uncracked case").

The results of the cracked case are presented in Fig.17, and the net pressure (PM(UC)) of the uncracked case is also shown in this figure as a black dashed line. It is founded that due to the reduction of stiffness, the net pressures (PM(UC)) in the uncracked case exceeded those obtained in the cracked case (PM(C)) over the entire pile. This made the inversion results of the cracked case more closely fit the actual pressure over 6 – 8 m depth, while less accurately fitting the actual pressures over 0 – 3 m depth. Overall, R^2 of the results in the cracked case was 0.69. Both inversion results were broadly consistent with the actual net pressures, indicating that non-linear reduction of bending stiffness of the pile can be ignored in this filed case.

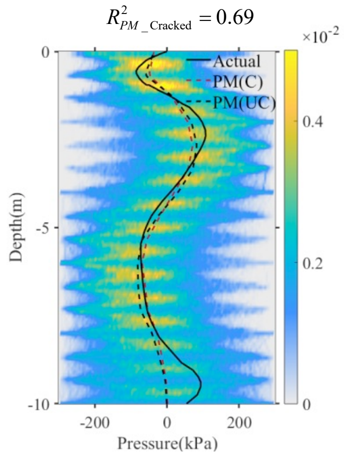

Fig. 17. Inversion results of the cracked case (Note: PM=posterior mean; C=cracked; UC=uncracked, using the results from Fig. 12f).

However, it is important to acknowledge that in cases involving highly non-linear structural behavior, such as load inversion on largely deformed tunnel structures mentioned in the introduction section, ignoring non-linear behavior may introduce significant bias in the results. Moreover, non-linear behavior necessitates an iterative solution of the forward model, resulting in computational costs that are a product of the number of iterations in the forward model and the number of Markov Chain steps. This can be time-consuming and pose challenges in achieving convergence in our approach. Hence, further research is warranted to address this limitation. It should also be noted that in this study, we assumed that the model error was negligible compared to the measurement error. Therefore, the likelihood function only accounted for the measurement error. The satisfactory inversion results obtained imply that this assumption is acceptable in this simple field case. However, it is possible that the model error could have an impact on the inversion results, particularly in cases where the physical process exhibits high non-linearity. Therefore, in future work, it might be worthwhile to consider the model error in order to enhance the accuracy of the inversion results.

The computational cost of the filed case provides a reference for the potential extension to non-linearity. Although the forward model is simple and linear, a dense FEM mesh was used with 101 elements spaced at 0.1 m. Accurate estimation of the posterior distribution for calculations A−F was achieved with Markov chains of length 10000. Using a desktop with a Ryzen 9, 12-Core, 3.8GHz Processor, the DE-MC for calculations A−F, with n values of 4, 8, 12, 14, 15, and 16, took 27.9, 56.6, 83.0, 96.9, 103.9 and 109.4 seconds, respectively. This low computational cost suggests that one should be able to extend this approach to nonlinear cases in the near future. However, improving efficiency of the MCMC sampling method is also an urgent consideration [34].

5 Conclusions

A Bayesian inversion approach is presented to identify the earth pressures on in-service underground structures using structural deformation data. This approach offers a natural regularization advantage when input data is noisy or limited, as demonstrated by the following:

i) When deformation data is contaminated by measurement errors, deterministic inversion can result in ill-conditioning. However, the posterior mean of the Bayesian approach flattens ill-conditioned features of individual solutions and identifies the actual pressures well with no need for explicit regularization.

ii) The posterior distribution in the Bayesian approach recognizes and quantifies non-uniqueness probabilistically. This property is particularly valuable in underdetermined cases, where a solution cannot be uniquely determined. The numerical example demonstrates that this approach yields relatively good inversion results even when the number of unknown parameters is slightly larger than that of the observed data.

This approach has been applied to a recorded field case to infer net pressures on a pile. The actual recorded pressures fit well with the inversion results, indicating effectiveness of this approach in practical engineering.

It is worth mentioning that all cases presented in this paper are linear and classical. Further extensions to non-linear mechanical systems (such as highly deformed tunnel structures) are of great interest. The small computational cost in the current applications suggests that such extensions can be feasible. Certainly, improving the statistical and computational efficiency of MCMC algorithm and considering model errors in the likelihood function are also urgent.

APPENDIX A: LINEAR INTERPOLATING VECTOR

This appendix presents the commonly-used linear interpolating vector $\mathbf{I_Z}(z)$:

$$q(z) = \mathbf{I_Z}(z)\mathbf{x} \tag{A1}$$

where q contains n-1 pieces of the linear functions on intervals $[z_i, z_{i+1}]$ (i=1,…,n-1), and vector $\mathbf{x}$ contains n unknown nodal values $(x_1,x_2,\ldots,x_n)^{\mathrm{T}}$. Coordinate of the nodes is denoted by $\mathbf{z}=(z_1,z_2,\ldots,z_n)^{\mathrm{T}}$, and spacing between the nodes by $\Delta s_i = z_{i+1} - z_i$.

The linear interpolant for q at z can be written as:

$$q(z) = \sum_{i=1}^{n-1} a_i x_i + b_i x_{i+1} \tag{A2}$$

where,

$$a_i = \begin{cases} \dfrac{z_{i+1} - z}{\Delta s_i} & z_i \le z \le z_{i+1} \\ 0 & else \end{cases}, \tag{A3}$$

$$b_i = \begin{cases} \dfrac{z - z_i}{\Delta s_i} & z_i \le z \le z_{i+1} \\ 0 & else \end{cases}, \tag{A4}$$

For mathematical convenience, matrix is adopted, and thus:

$$\mathbf{I_z}(z) = (1, \dots, 1)_{1\times(n-1)} \begin{bmatrix} a_1 & b_1 & & & \\ & a_2 & b_2 & & \\ & & \ddots & & \\ & & & a_{n-1} & b_{n-1} \end{bmatrix}_{(n-1)\times n} \tag{A5}$$

APPENDIX B: "BEAM ON ELASTIC FOUNDATION" MODEL

The partial differential governing functions of "beam on elastic foundation" model can be described as

$$EI(z)\frac{d^4 y}{dz^4} + k(z)y = q(z) \tag{B1}$$

where EI is the flexural rigidity of the beam that may vary with depth z, y represents the deflection function of the beam. $k(z)y$ is the reaction of the foundation, and k is the foundation stiffness. q is the pressure field determined by load parameters **x** (Eq. A1).

Discretization of (B1) using finite element method:

$$\mathbf{d}' = \mathbf{K}^{-1}\mathbf{f}(\mathbf{I_z}(z)\mathbf{x}) \tag{B2}$$

Where **d'** is the predicted deformation vector under pressure field q. **f** is a vector-valued function where **f** ($\mathbf{I_z}(z)\mathbf{x}$) is equivalent to q (i.e., $\mathbf{I_z}(z)\mathbf{x}$) with the transformation rules of virtual work. **K** is the global stiffness matrix that is assembled by element stiffness matrix $\mathbf{k}^e$, consisting two parts:

$$\mathbf{k}^e = \mathbf{k}_b + \mathbf{k}_f$$

Where $\mathbf{k}_b$ represents beam stiffness matrix. $\mathbf{k}_f$ is closely resembles the beam mass matrix due to the term $k(z)y$ in (B1). Derivation of them has been presented in Griffiths [35]:

$$\left. \begin{aligned} k_{b(ij)} &= \int_{z_e}^{z_e+L} EI(z)\frac{d^2 N_i}{dz^2}\frac{d^2 N_j}{dz^2}dz \\ k_{f(ij)} &= \int_{z_e}^{z_e+L} k(z)N_i N_j dz \end{aligned} \right\} i, j = 1, 2, 3, 4 \tag{B3}$$

where L is the length of an individual beam element, z_e is the coordinate of element e, $\xi = z - z_e$, and

$$\begin{aligned} N_1 &= \frac{2}{L^3}\xi^3 - \frac{3}{L^2}\xi^2 + 1, \quad N_2 = \frac{1}{L^2}\xi^3 - \frac{2}{L}\xi^2 + \xi \\ N_3 &= -\frac{2}{L^3}\xi^3 + \frac{3}{L^2}\xi^2, \qquad N_4 = \frac{1}{L^2}\xi^3 - \frac{1}{L}\xi^2, \end{aligned} \tag{B4}$$

f is also assembled by element forces $\mathbf{f}^e(\mathbf{I_z}(z)\mathbf{x})$ that is equivalent to the pressures q with the transformation of virtual work equation:

$$\mathbf{f}^e(\mathbf{I}_\mathbf{z}(z)\mathbf{x}) = \begin{bmatrix} 1 & 0 & -\frac{3}{L^2} & \frac{2}{L^3} \\ 0 & 1 & -\frac{2}{L} & \frac{1}{L^2} \\ 0 & 0 & \frac{3}{L^2} & -\frac{2}{L^2} \\ 0 & 0 & -\frac{1}{L} & \frac{1}{L^2} \end{bmatrix} \begin{Bmatrix} F_{p0} \\ F_{p1} \\ F_{p2} \\ F_{p3} \end{Bmatrix} \tag{B5}$$

where,

$$\begin{aligned} F_{p0} &= \int_{z_e}^{z_e+L} q(z)dz = \int_{z_e}^{z_e+L} \mathbf{I}_\mathbf{z}(z)\mathbf{x}dz \qquad F_{p1} = \int_{z_e}^{z_e+L} q(z)\xi dz = \int_{z_e}^{z_e+L} \mathbf{I}_\mathbf{z}(z)\mathbf{x}\xi dz \\ F_{p2} &= \int_{z_e}^{z_e+L} q(z)\xi^2 dz = \int_{z_e}^{z_e+L} \mathbf{I}_\mathbf{z}(z)\mathbf{x}\xi^2 dz \quad F_{p3} = \int_{z_e}^{z_e+L} q(z)\xi^3 dz = \int_{z_e}^{z_e+L} \mathbf{I}_\mathbf{z}(z)\mathbf{x}\xi^3 dz \end{aligned} \tag{B6}$$

Acknowledgements

This study was supported by Natural Science Foundation of China (Grant No. 51978523). A.L. acknowledges support from Engineering and Physical Sciences Research Council under the CoSInES (EP/R034710/1). Z.T. acknowledges support from China Scholarship Council.

Data Availability Statement

All data generated or used during the study are included in this paper. Code that supports the findings are available from tianzy@tongji.edu.cn upon reasonable request, including MATLAB script for FEM forward model and DE-MC sampling algorithm.

Declarations

Conflict of interest The authors declare that they have no conflict of interest.

References

[1] Zhang D., Liu Z., Wang R., Zhang D. Influence of grouting on rehabilitation of an over-deformed operating shield tunnel lining in soft clay. Acta Geotechnica. 2019; 14: 1227–1247.

[2] Tian Z., Xu P., Gong Q., Zhao Y., Zhou S. Health-degree model for stagger-joint-assembled shield tunnel linings based on diametral deformation in soft-soil areas. Journal of Performance of Constructed Facilities. 2023; 37(3): 04023019.

[3] Massarsch K. R. New method for measurement of lateral earth pressure in cohesive soils. Canadian Geotechnical Journal. 1975; 12: 142–146.

[4] Han L., Ye G. L., Li Y. H., Xia X. H., Wang J. H. In-situ monitoring of frost heave pressure during cross passage construction using ground freezing method. Canadian Geotechnical Journal. 2016; 53: 530–539.

[5] Zhao Y., Zhu Z., Liu W., Zhan J., Wu D. Application of 3D laser scanning on NATM tunnel deformation measurement during construction. Acta Geotechnica. 2022. https://doi.org/10.1007/s11440-022-01546-0.
[6] Yan Q., Zhang W., Zhang C., Chen H., Dai Y., Zhou H. Back analysis of water and earth loads on shield tunnel and structure ultimate limit state assessment: a case study. Arabian Journal for Science & Engineering. 2018; 44: 4839–4853.
[7] Mashimo H., Ishimura T. Evaluation of the load on shield tunnel lining in gravel. Tunnelling and Underground Space Technology. 2003; 18: 233–241.
[8] Li X., Zhou S., Di H. Observed ground pressure acting on the lining of a large-diameter shield tunnel in sandy stratum under high water pressure. Advances in Civil Engineering. 2020; https://doi.org/10.1155/2020/3091528.
[9] Gioda G., Jurina L. Numerical identification of soil-structure interaction pressures. International Journal for Numerical and Analytical Methods in Geomechanics. 1981; 5(1), 33–56.
[10] Liu R., Dobriban E., Hou Z., Qian K. Dynamic load identification for mechanical systems: a review. Archives of Computational Methods in Engineering. 2021; https://doi.org/10.1007/s11831-021-09594-7.
[11] Sanchez J., Benaroya H. Review of force reconstruction techniques. Journal of Sound & Vibration. 2014; 333(14): 2999–3018.
[12] Parker R. L. Understanding inverse theory. Annual Review of Earth and Planetary Sciences. 1977; 5: 53–64.
[13] Liu Q., Liu H., Huang X., Pan Y., Luo C., Sang H. Inverse analysis approach to identify the loads on the external TBM shield surface and its application. Rock Mechanics and Rock Engineering. 2019; 52: 3241–3260.
[14] Liu H., Liu Q., Liu B., Tang X., Ma H., Pan Y., Fish J. An efficient and robust method for structural distributed load identification based on mesh superposition approach. Mechanical Systems and Signal Processing. 2021; 151: 107383.
[15] Wei Y., Xie P., Zhang L. Tikhonov regularization and randomized GSVD. SIAM Journal on Matrix Analysis and Applications. 2016; 37(2): 649–675.
[16] Bodin, T., Sambridge M., Gallagher K. A self-parametrizing partition model approach to tomographic inverse problems. Inverse Problems. 2009; 25(5): 55009–55030.
[17] Han L, Wang L, Zhang W., Chen Z. Quantification of statistical uncertainties of unconfined compressive strength of rock using Bayesian learning method. Georisk. 2021; 16(1): 37-52.
[18] Yang H., Zhang L., Li D. Efficient method for probabilistic estimation of spatially varied hydraulic properties in a soil slope based on field responses: A Bayesian approach. Computers and Geotechnics. 2018; 102: 262-272.
[19] Zhang W., Wu C., Zhong H., Li Y., Wang L. Prediction of undrained shear strength using extreme gradient boosting and random forest based on Bayesian optimization. Geoscience Frontiers. 2021; 12(1): 469-477.
[20] Qin H., Vrugt J. A., Xie X., Zhou Y. Improved characterization of underground structure defects from two-stage Bayesian inversion using crosshole GPR data. Automation in Construction. 2018, 95: 233-244.
[21] Li Q., Lu Q. A hierarchical Bayesian method for vibration-based time domain force reconstruction problems. Journal of Sound and Vibration. 2018; 421, 190–204.
[22] Zhang E., Antoni J., Feissel P. Bayesian force reconstruction with an uncertain model. Journal of Sound & Vibration. 2012; 331(4): 798–814.
[23] Aucejo M., Smet, O. D. On a full Bayesian inference for force reconstruction problems. Mechanical Systems and Signal Processing. 2018; 104, 36–59.

[24] Aucejo M., Smet, O. D. An optimal Bayesian regularization for force reconstruction problems. Mechanical Systems and Signal Processing. 2019; 126: 98–115.
[25] Li Q., Lu Q. A revised time domain force identification method based on Bayesian formulation. International Journal for Numerical Methods in Engineering. 2019; 118, 411–431.
[26] Robert C. P. The Bayesian Choice: From Decision-Theoretic Foundations to Computational Implementation, 2nd edition. New York: Springer; 2007.
[27] Metropolis N., Rosenbluth A. W., Rosenbluth M. N., Teller A. H., Teller E. Equations of state calculations by fast computing machines. Journal of Chemical Physics. 1953; 21: 1087–1091.
[28] Wang L., Xiao T., Liu S., Zhang W., Yang B., Chen L. Quantification of model uncertainty and variability for landslide displacement prediction based on Monte Carlo simulation. Gondwana Research. 2023. https://doi.org/10.1016/j.gr.2023.03.006.
[29] Ter Braak C. J. F. A Markov Chain Monte Carlo version of the genetic algorithm Differential Evolution: easy Bayesian computing for real parameter spaces. Statistics & Computing. 2006; 16(3): 239–249.
[30] Gelman A., Rubin D. B. Inference from iterative simulation using multiple sequences. Statistical Science. 1992; 7(4), 457–472.
[31] Draper N. R. and Smith H. Applied Regression Analysis, 2nd edition. New York: Wiley; 1981.
[32] Smethurst J. A., and Powrie W. Monitoring and analysis of the bending behaviour of discrete piles used to stabilise a railway embankment. Géotechnique. 2007; 57(8): 663–677.
[33] Xu SY., Lawal A.I., Shamsabadi A. Taciroglu E. Estimation of static earth pressures for a sloping cohesive backfill using extended Rankine theory with a composite log-spiral failure surface. Acta Geotechnica. 2019; 14: 579–594.
[34] Karagiannis G., Andrieu C. Annealed importance sampling reversible jump MCMC algorithms. Journal of Computational and Graphical Statistics. 2013; 22(3): 623–648.
[35] Griffiths D. V. Advantages of consistent over lumped methods for analysis of beams on elastic foundations. Communications in Applied Numerical Methods. 1989; 5(1): 53–60.